Two highstands during the Last Interglacial: insights from palaeoshorelines and marine terraced deposits of ionian coast of Apulia (southern Italy)

Vincenzo De Santis[a*], Paolo Montagna[b], Giovanni Scicchitano[a], Giuseppe Mastronuzzi[a], Edwige Pons-Branchu[c], Giovanni Scardino[a], José E. Ortiz[d], Yolanda Sánchez-Palencia[d], Trinidad Torres[d], Massimo Caldara[a]

EGU General Assembly 2024 — Sharing is encouraged
UNIVERSITÀ DEGLI STUDI DI BARI ALDO MORO — DIPARTIMENTO DI SCIENZE DELLA TERRA E GEOAMBIENTALI — DISTEGEO

1) DATA AND RESULTS

Field data and chronological analyses using U-Th dating as well as amino acid racemization (AAR) methods allowed for the identification and dating of three terraced deposits (TD) as well as their related palaeoshorelines (PS) along the Ionian coast of the Apulia region, southern Italy (De Santis et al., in press). In descending order of elevation, they are (Figs 1 and 2; Table 1):

-Terraced Deposit 1 (TD1) and Palaeoshoreline 1 (PS1, located at +40 ± 5), dated to marine isotope stages 7-8 (MIS 7–8).

-Terraced Deposit 2 (TD2; Figs 3-6), characterised by five sub-units (from TD2-su1 to TD2-su5; see Tab. 1) marking a transgressional episode and the first MIS 5.5 highstand. The sub-unit which marks an earlier phase of transgression (TD2-su1), was found to have an age of ~128 ky BP using U-Th dating. AAR analyses revealed an age of 128.4±26.2 ky BP for one of the sub-units marking the later stages of transgression (TD2-su3) and aminozone E (MIS 5.5) for one of the sub-units marking the highstand (TD2-su4); *Thetystrombus latus* (Gmelin) was also found within this latter unit.

-Palaeoshoreline 2 (PS2; located at +30 ± 2 m), present at the inner margin of TD2 and associated with the first, higher elevation MIS 5.5 highstand.

-Terraced Deposit 3 (TD3; Figs 7, 8), which marks the occurrence of a second, lower elevation MIS 5.5 highstand, can be subdivided into two sub-units TD3-su1 and TD3-su2 (Tab.1), lying one over another in continuous segmentation. AAR analyses revealed that TD3-su2 corresponds to aminozones E–D (MIS 5.5-MIS 5.3). It was also found to have an age of 122.49 ± 1.25 ky BP using U-Th dating.

-Palaeoshoreline 3 (Ps3; located at +19 ± 2 m), present at the inner margin of TD3 and associated with the second, lower elevation MIS 5.5 highstand that occurred ~122 ky BP.

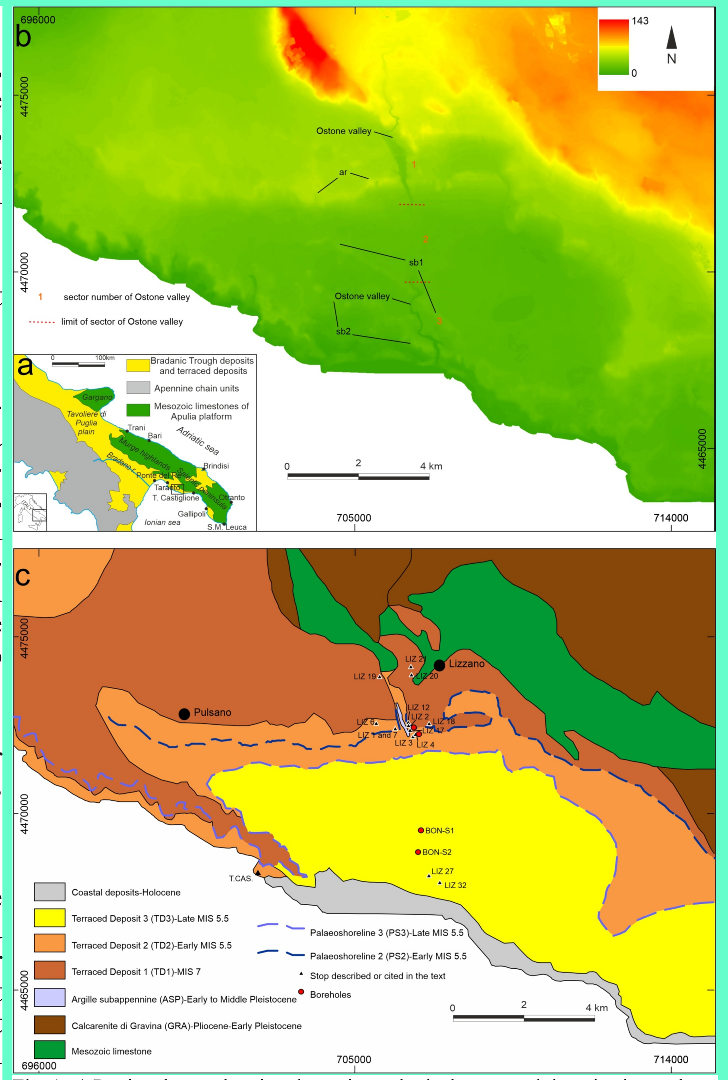

Fig. 1. a) Regional map showing the main geological-structural domains in southern Italy. b) Digital elevation model (DEM) of the study area; ar: relict aeolian ridge (see main text for more details); sb1 and sb2: relict sandy bars (see main text for more details); red numbers and red dotted lines represent the sectors of the Ostone valley and their boundaries, respectively. c) Schematic geological map of the study area.

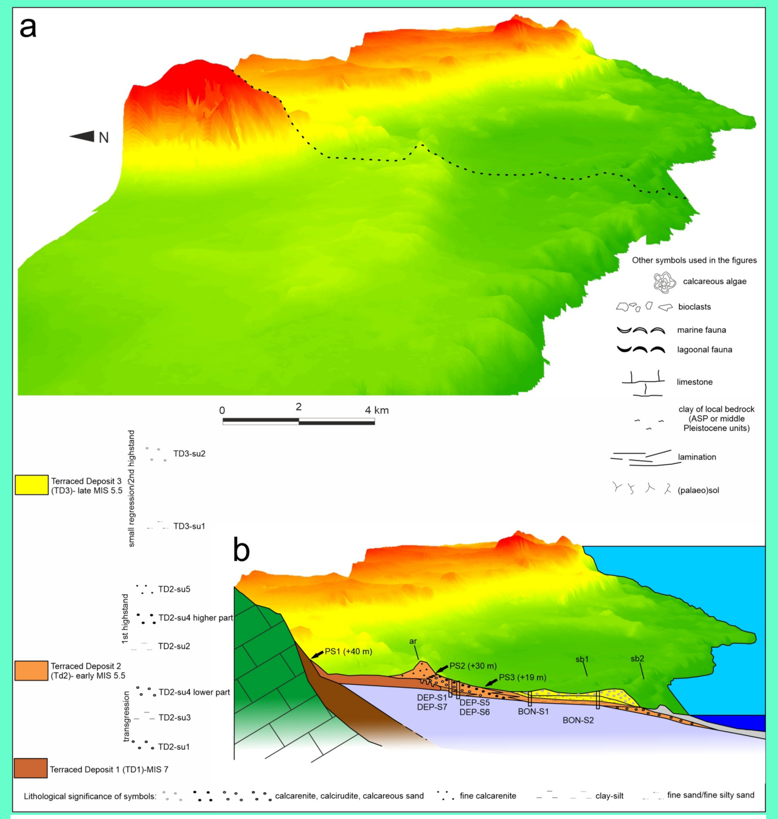

Fig. 2. a) 3D reconstruction of the study area; the colours represent their elevation above present-day sea level (see the upper-right box in Fig. 1b). The black dotted line represents the trace of the section presented in 2b. b) Conceptual geological section showing the terraced deposits (TD1, TD2, and TD3) and the elevation above present-day sea level of their associated palaeoshorelines (PS1, PS2, and PS3). The position of boreholes from which stratigraphic samples were recovered (DEP-S1, DEP-S7, DEP-S5, DEP-S6, BON-S1, and BON-S2) are also reported. Note that the symbols used for the coloured fields of TD2 and TD3 represent their lithological and depositional characteristics. The four symbols given for three lithologies (calcarenite, chalcirudite, and calcareous sand) indicate that each of the four symbols can represent calcarenite, chalcirudite, or calcareous sand without any specification. This distinction in the symbolism indicates the unit and depositional context (transgression or highstand) of the three lithologies, as indicated in the rest of the legend. The same symbols are used in following figures.

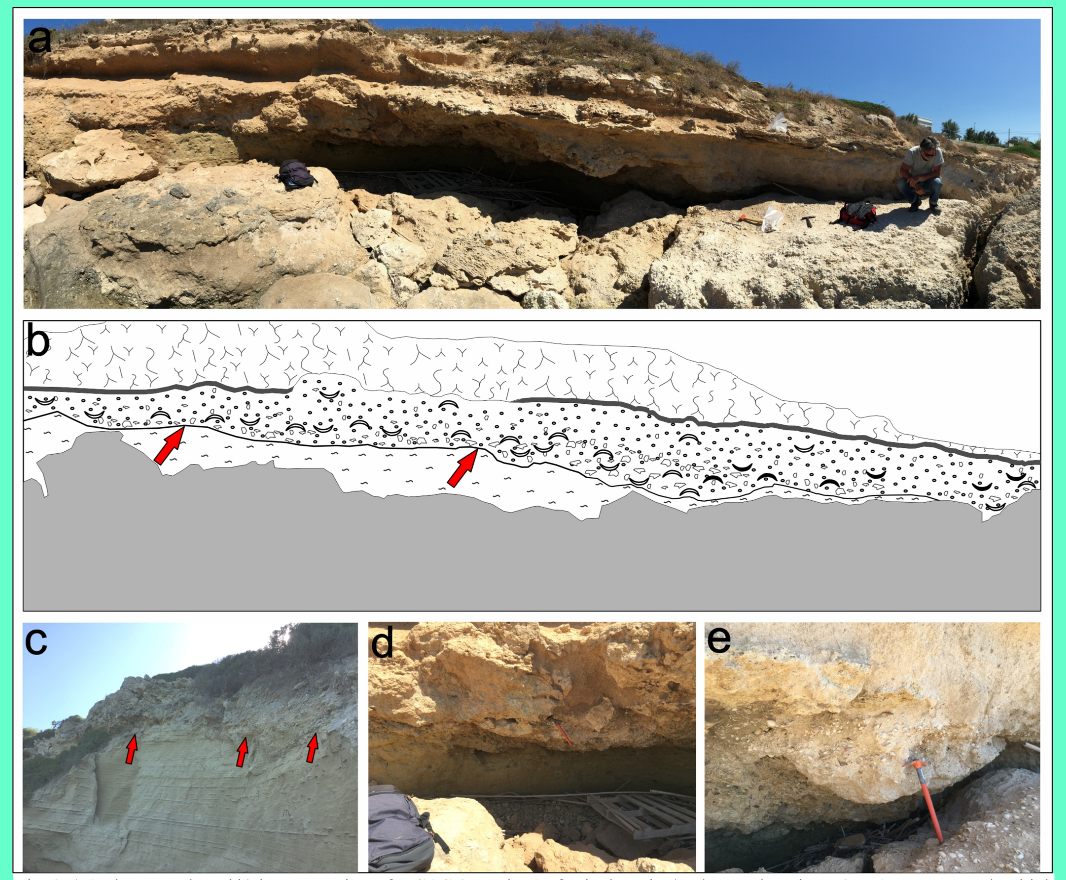

Fig. 3 a) A photograph and b) interpretation of T.CAS (see Fig. 1c for its location) where sub-unit TD2-su1 crops out. The thick line and red arrows show the abrupt, erosive contact that characterises the transgression surface of TD2-su1 on the local bedrock (either ASP or another undefined middle Pleistocene unit). Note that all samples initialled with “T.CAS-U1” (see Table 1) originate from TD2-su1 but have not been reported in this figure because they did not come from the section presented here. In Fig. 4b, the light grey colour indicates both blocks detached from the cliff and are now tilted, with some limestone blocks likely belonging to an older indeterminate substrate embedded within TD2-su1. The dark grey colour indicates the thin arenaceous layer younger than TD2-su1. c) On the western side of the Torre Castelluccia headland, the transgression of TD2-su1 above the silty-clayey termination of the local bedrock is clearly visible, while the transgressional surface (indicated with red arrows) can be clearly observed to extend from present sea level to +15–17 m. d) A close-up of the transgressional surface. e) A close-up of a highly fossiliferous layer within TD2-su1.

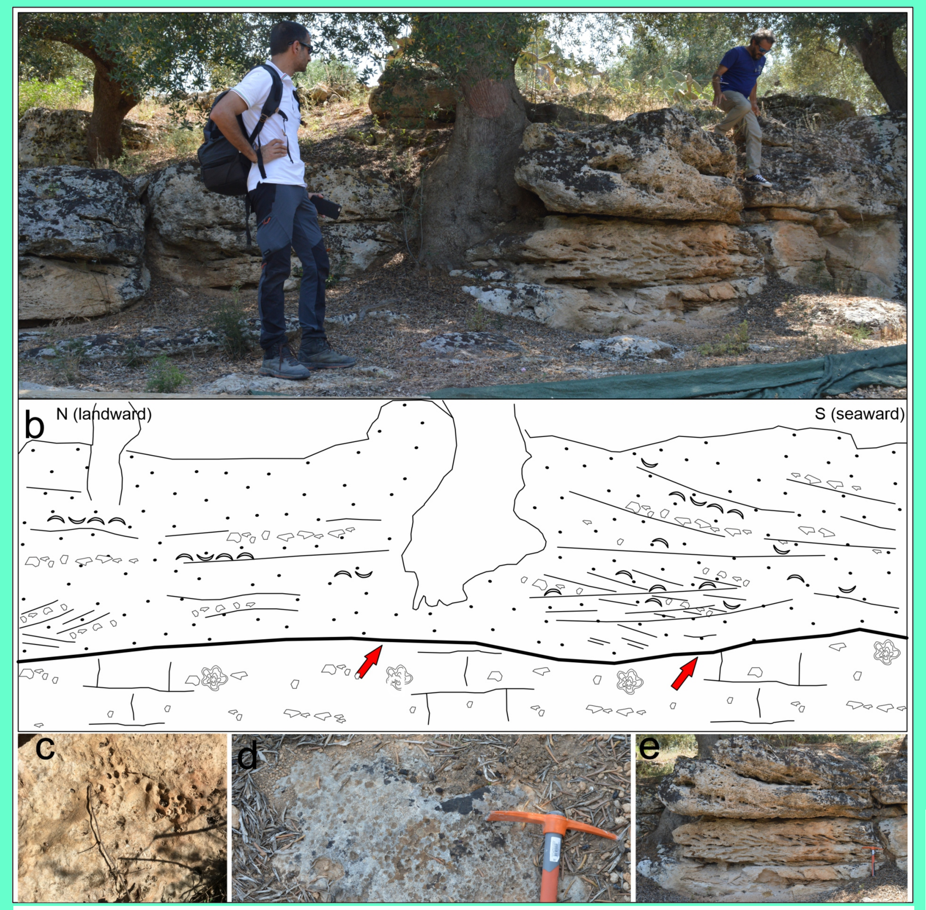

Fig. 4. a) A photograph and b) interpretation of stop LIZ2 (see Fig. 1c for its location), showing the inner margin of TD2 (sub-unit TD2-su4) in pinch out above the underlying TD1. TD2 represents the transgression of MIS 5.5 above TD1; the transgression surface is marked by a thick line and red arrows. c) Stop LIZ7 (see Fig. 1c for its location): detailed look at the transgression surface at the top of TD1 with traces of *Gastrochaenolites cor* (Bromley and D'Alessandro, 1987) with the original borer marine bivalve *Petricola lithophaga* (Retzius). d) Lithophagid holes on the surface transgression at the top of TD1 (stop LIZ2). e) Detailed photograph of the cross-stratified laminations within TD2 (see Section 4.2).

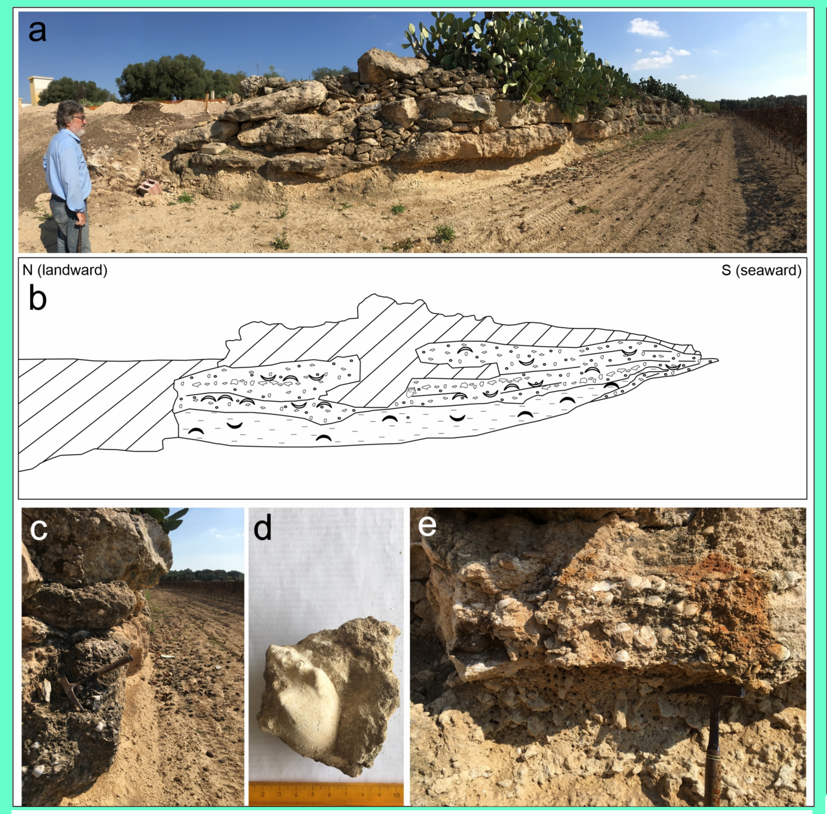

Fig.5. a) A photograph and b) interpretation of stop LIZ3 (see Fig. 1c for its location) showing the interdigitation between the lower sub-unit TD2-su3 and sub-unit TD2-su4, which is visible at meter-scale. c) A detailed record of the site and the in situ *Thetystrombus latus* (Gmelin) specimen. d) Close-up of T. latus after sampling. e) Close-up of the contact between the underlying sub-unit TD2-su3, which contains specimens of *Cerastoderma glaucum* (Bruguiere), and the overlying sub-unit TD2-su4, which is rich in bivalves (mainly *Glycymeris* spp).

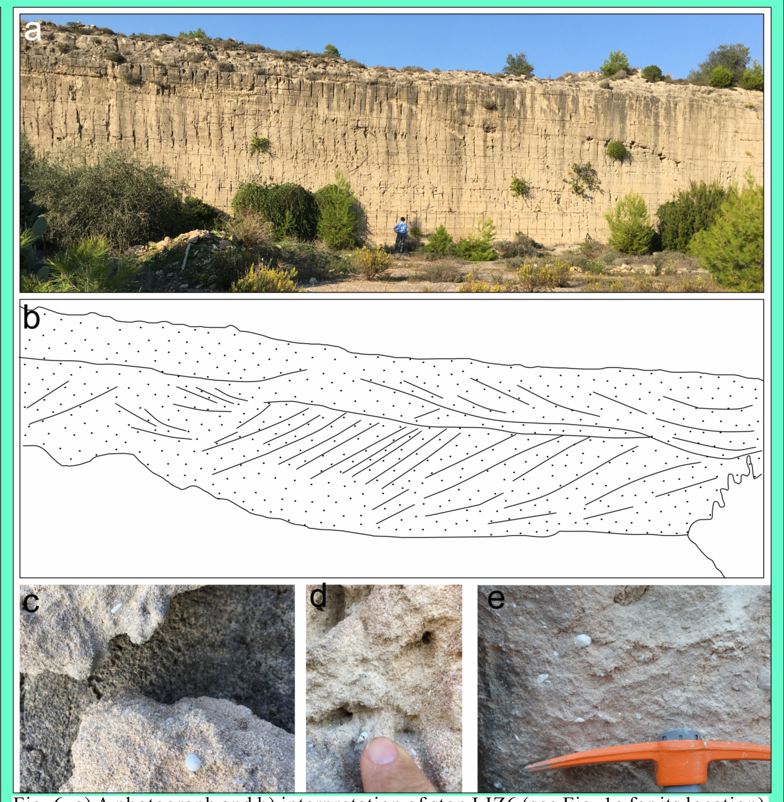

Fig. 6. a) A photograph and b) interpretation of stop LIZ6 (see Fig. 1c for its location), where the fossil coastal dune of sub-unit TD2-su5 outcrops. c) and d) Close-ups of continental pulmonated gastropods present in the aeolian sands. e) Layers of coarser calcarenites with marine mollusc shells visible at the southern edge of the quarry.

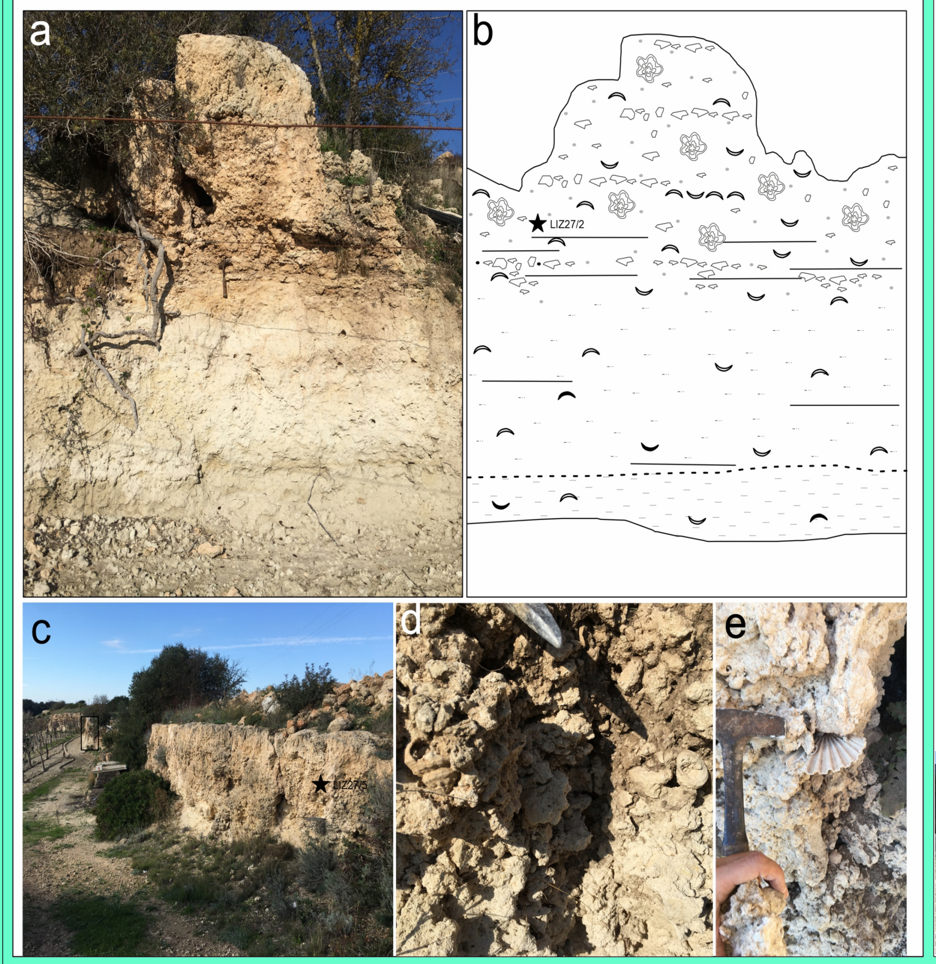

Fig. 7. a) photograph and b) interpretation of stop LIZ27 (see Fig. 1c for its location), where TD3 outcrops; this unit is composed of the lower sub-unit TD3-su1 and the upper TD3-su2. TD3 overlies TD2-su2. c) Overview of the steep flank of the Ostone valley in Sector 3 (Fig. 1a), where the section of LIZ27 reported in a) and b) was measured (black square). The black stars indicate the locations from which samples LIZ27/2 and LIZ27/5 were collected (Table 1). d) Specimens of *B. rugosa* that are abundant in TD3-su2. e) Specimen of *P. jacobaeus* within TD3-su2.

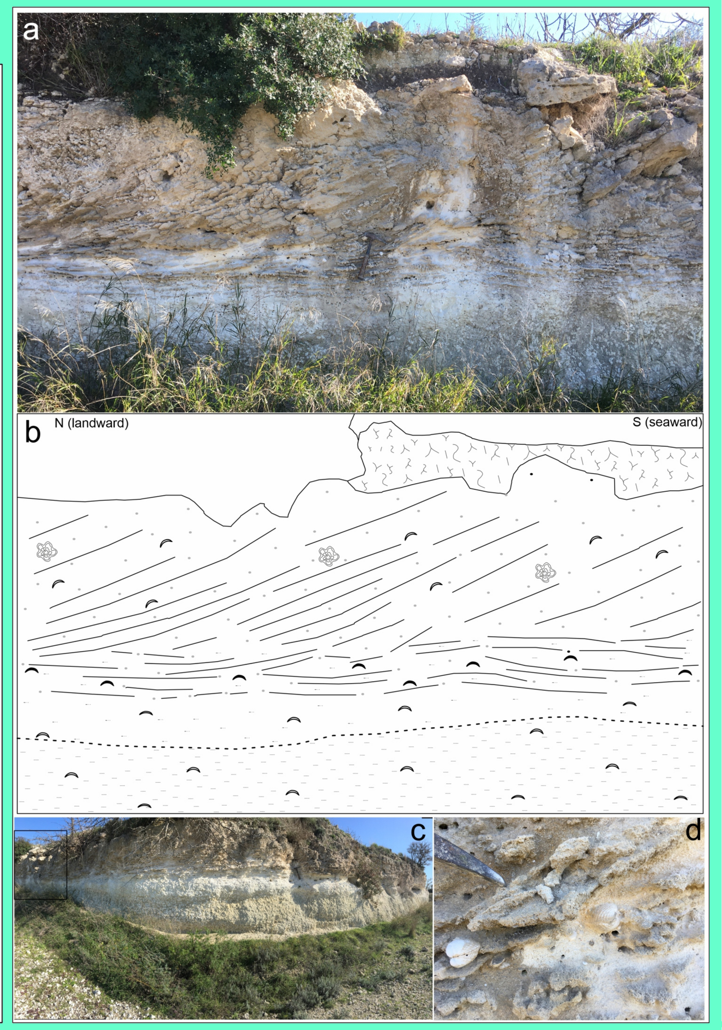

Fig. 8. a) photograph and b) interpretation of locality LIZ32 (see Fig. 1c for its location), where TD3 outcrops. TD3 overlies TD2-su2. c) Overview of the outcrop where section LIZ32 was measured (black square). d) Close-up of the transition between TD3-su1 and TD3-su2, which contains specimens of *C. glaucum*.

Teraced deposit	Associated palaeoshoreline with its elevations in metres above the present sea level (a.p.s.l.)	Facies of terraced deposit	Depositional environment	Depositional context	Samples analysed with Aminozone (capital letter) or numerical age (ky BP)	Dated material and dating method	MIS
TD1	PS1 (40±5)	Not recognised	high to moderate energy submerged beach	Not defined	LIZ19/1: 264.28 ±5.71	*Cladocora caespitosa* (U/Th)	7-8
					LIZ18/1:194.81±1.16	*Alocyathus* sp. (U/Th)	
TD2	PS2 (30±2)	TD2-su5	aeolian coastal dune	highstand			early 5.5
		TD2-su4	high energy beach, from backshore to shoreface.	transgression in the lower part highstand in the upper part	LIZ17a: aminozone E	*Glycymeris pilosa.* (Amino acid racemization)	
					LIZ17b: aminozone E	*Glycymeris pilosa* (Amino acid racemization)	
		TD2-su3	lagoon	transgression	LIZ4a: 128.4±26.2	*Cyprideis torosa* (Amino acid racemization)	
		TD2-su2	low energy environment; offshore	highstand			
		TD2-su1	high to moderate energy submerged beach passing laterally to more protected environments and upwards to nearshore/offshore transition	transgression	T.CAS-U1/1: 127.851±1.47	*Cladocora caespitosa* (U/Th)	
					T.CAS-U1/a: aminozone E-D	*Glycymeris pilosa* (Amino acid racemization)	
					T.CAS-U1/b: aminozone E	*Bolma rugosa* (Amino acid racemization)	
					T.CAS-U1/c: aminozone E	*Arca noae* (Amino acid racemization)	
TD3	PS3 (19±2)	TD3-su2	infralittoral beach environment under the influence of bottom currents	highstand	LIZ 27/2: aminozone E-D	*Glycymeris pilosa* (Amino acid racemization)	late 5.5
					LIZ 27/5: 122.49 ±1.25	*Alocyathus* sp. (U/Th)	
		TD3-su1	lower energy protected environment	highstand			

Table 1. List of identified terraced deposits with identified sub-units, associated palaeoshorelines, samples, aminozones, numerical ages, and their corresponding MISs. Note that the first part of the sample ID (the 6th column) indicates the locality from which the sample was collected; for example, sample LIZ18/1 was collected at locality LIZ18 (see Fig. 1c for the position of each locality).

2) DISCUSSION-RSL TREND RECONSTRUCTION

We focused on the palaeoshorelines and deposits of the LIG (PS2 and TD2; PS3 and TD3).
PS2 is associated with the first highstand of MIS 5.5. The age ranging between 127.851 ± 1.47 and 128.4 ± 26.2 ky BP from sub-units of TD2 marking the transgression, suggests that the transgression towards this first highstand was still occurring at ~128 ky BP.
PS3 is associated with the second highstand of MIS 5.5 and has an age of ~122 ky BP, based on data from TD3.
Also considering the above-mentioned constraints and since it was not possible to obtain an absolute age for the TD2 sub-units which mark the first MIS 5.5 highstand, we considered the following two scenarios (Kopp et al., 2013):
1) Scenario 1, which assumes that the first highstand of MIS 5.5 occurred at 125 ky Bp;
2) Scenario 2, which assumes that the first highstand of MIS 5.5 occurred at 123 ky BP.
In both scenarios, we assumed a mean sea level value of +7.5 ± 1.5 m during the first highstand of MIS 5.5. We then calculated the uplift rate of PS2 for both scenarios, assuming a constant uplift rate to the present day.
These uplift rates were used to calculate (Fig. 9) the position of PS3 at 122.49 ± 1.25 (rounded at ~122 ky BP) as well as the position of the dated layer of the lowest transgressive sub-unit of TD2 found at an elevation of +3.80 m, dated at 127.851 ± 1.47 ky BP (rounded at ~128 ky BP), with the latter assumed to have been deposited at a water depth of 5–10 metres.

Both scenarios give an uplift rate of 0.18 ± 0.03 mm/yr.
The mean elevation of PS3 at the time of its formation (i.e., the sea level at ~122 ky BP, corresponding to the second highstand of MIS 5.5) was calculated to be -2.96 and -3.32 m for Scenarios 1 and 2, respectively (Fig. 9 a, b). After taking all uncertainties into account, the range of elevation of PS3 was found to be -2.96 ± 5.42 m for Scenario 1 and -3.32 ± 5.47 m for Scenario 2 (Fig. 9a, b).
We also calculated the position of the dated layer of the lowest transgressive sub-unit of TD2 (TD2-su1; ~128 ky BP) using the uplift rates obtained from the previous analysis and consequently, assuming a palaeo-water depth of 5–10 m, the sea-level at the same age, which was found to have a value of -11.79 ± 6.29 m (fig. 9a, b).
Although the mean RSL trend presented in this study were obtained from local data, they are consistent with other global and local MIS 5.5 sea-level reconstructions, which suggest the existence of two highstands, with the earlier highstand having a higher peak sea level than the second highstand (Kopp er al., 2013; Düsterhus et al., 2016; Rohling et al., 2019; Bini et al., 2020; De Santis et al., 2023).

We emphasise that the local RSL trend presented in this work (Fig. 9) is based on the interpretation of palaeoshorelines and related deposits found in the study area. Thus, this should be considered to be a broad RSL trend: we cannot rule out the possibility of minor sea-level oscillations that are not resolvable by the depositional and geomorphological record.

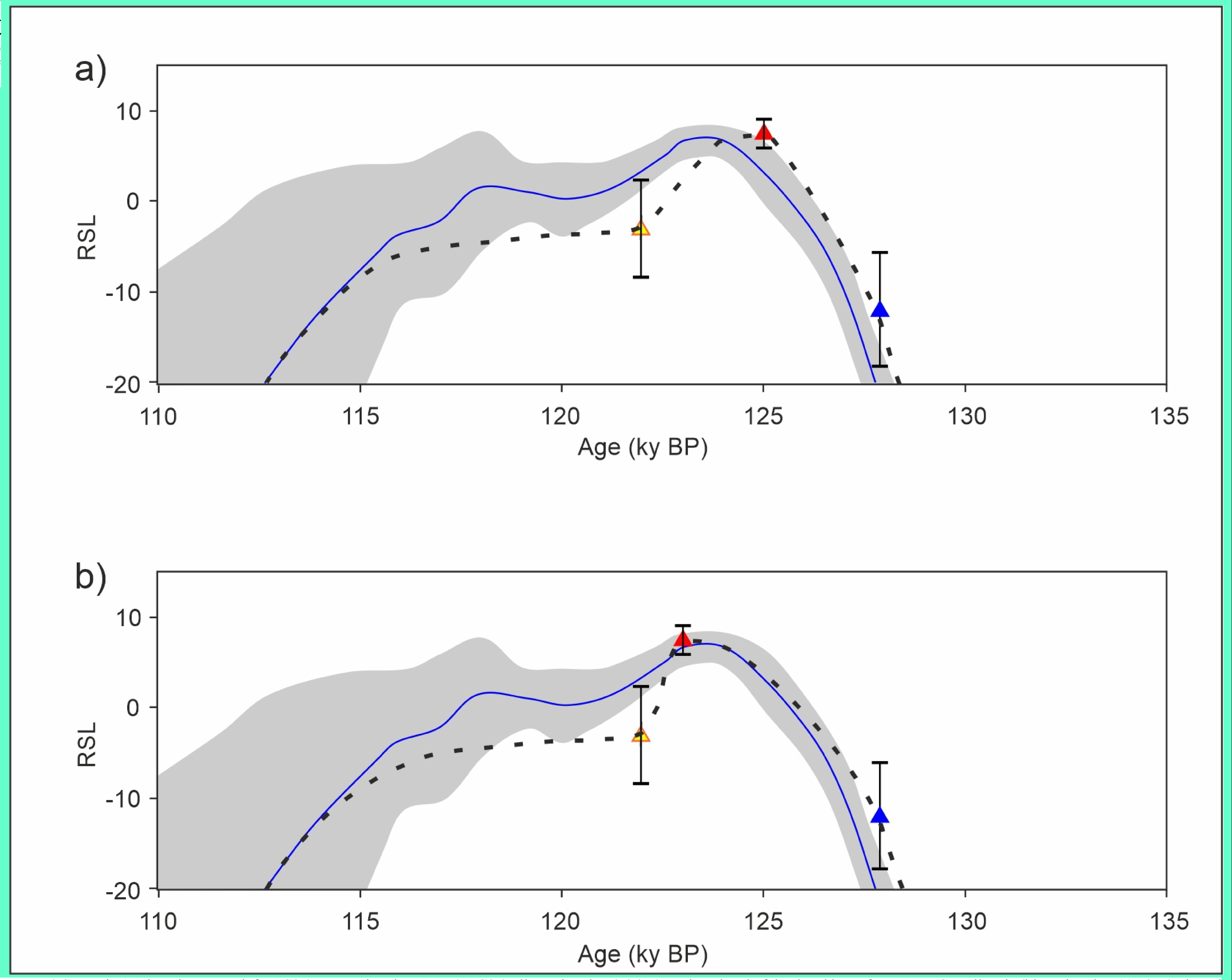

Fig. 9. Local highstands and RSL trends in the study area. a) Scenario 1: Elevations a.p.s.l. for PS2 (orange triangle; +7.5 m), PS3 (yellow triangle; -2.96 m), and sea level of the dated layer from Torre Castelluccia (blue triangle; -11.79 m) plotted along a resolved global mean sea level (GMSL) curve reported by Kopp et al (2013) (blue line); the 95% confidence intervals are indicated by the grey band. The dashed line represents a tentative reconstructed RSL trend for the study area based only on local geomorphological and chronological evidence. We emphasise that the local RSL trend should be considered to be a broad trend: we cannot rule out the possibility of minor sea-level oscillations that are not resolvable by the depositional and geomorphological record. The vertical bar on the yellow triangle represents the possible range of RSL values during the second highstand of MIS 5.5 (from -8.38 to +2.45 m). The vertical bar on the orange triangle represents the uncertainty of the elevation of the first sea-level highstand of MIS 5.5 (+6–9 m). The vertical bar on the blue triangle represents the uncertainty in the derived sea level obtained for the dated layer from Torre Castelluccia (from -5.5 to -18.08 m). b) Scenario 2: Same colour scheme as in a) but with the yellow triangle representing a value of -3.32 m and the vertical bar on the yellow triangle representing the entire range of possible RSL values for the second highstand during MIS 5.5 (from -8.79 to 2.15 m).

3) DISCUSSION-PALAEOCLIMATIC CONSIDERATIONS

In addition, we observed the presence of the marine gastropod *Bolma rugosa* (Linneo) and the absence of the marine gastropod *Thetystrombus latus* (Gmelin) in TD1, in the lowest transgressive sub-unit of TD2, and in TD3, and, conversely, the presence of T. latus and absence of *B. rugosa* in the upper sub-units of TD2 that mark the last phase of transgression and the first higher highstand of MIS 5.5 (Fig. 10, left). Based on the present-day distribution of these two species (Fig. 10, right) and the reconstructed RSL trend, we have tentatively identified, in a qualitative way, three climatic phases during MIS 5.5 (Fig. 11): 1) a first, warm-temperate/subtropical in the early MIS 5.5, characterised by the presence of *B. rugosa*; 2) a second, fully tropical, during the mid part of MIS 5.5, with a sea level at a mean value of ca. +7.5 ± 1.5 m and characterised by the presence of *T. latus* and disappearance of *B. rugosa*; 2) a third, again warm-temperate/subtropical, during the late MIS 5.5, characterised by the disappearance of *T. latus* and the reappearance of *B. rugosa*.

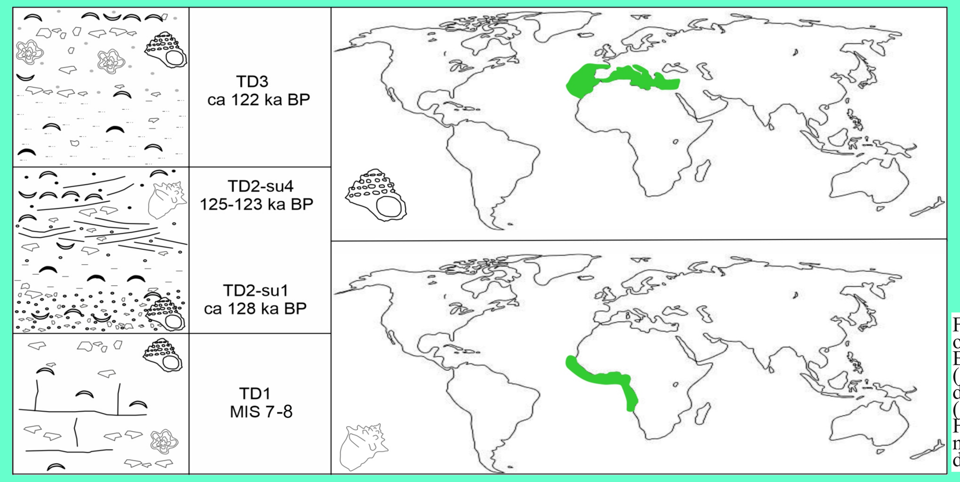

Fig. 10. Left: comprehensive schematic stratigraphy of the study area, showing the presence or absence of Bolma rugosa (Linneo) and Thetystrombus latus (Gmelin). Right: present-day geographical distribution of B. rugosa (upper panel) and T. latus (lower panel) from Global Biodiversity Information Facility data base (after removal of reports regarding no natural environment), which highlights the different hydroclimatic conditions of the two species.

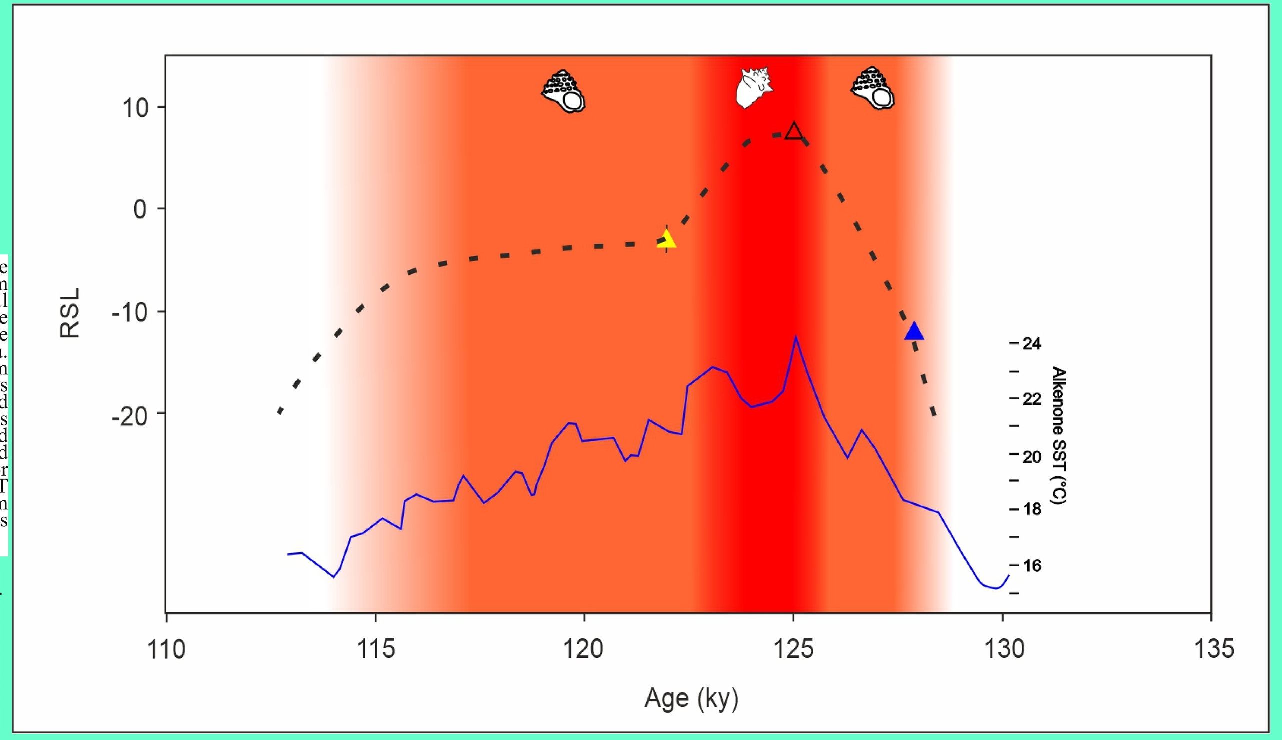

Fig. 11. Tentative reconstruction of the three climatc phases during MIS 5.5 inferred from our results. Red vertical band: tropical climatic phase characterised by the presence of *Thetystrombus latus* (Gmelin) and absence *Bolma rugosa* (Linneo) in the study area. Orange vertical bands: termperate to warm temperate/subtropical climatic phases characterised by the presence of *B. rugosa* and absence of *T. latus* in the study area. The bands representing climatic phases are plotted together with our reconstructed RSL-trend and data point in Scenario 1 (see Figure 9a for reference). The alkenone-based SST reconstruction by Kandiano et al. (2014) from the South Balearic Islands Basin (blue line) is plotted for comparison.

REFERENCES

-Bini M., Zanchetta G., Drysdale R.N., Giaccio B., Stocchi P., Vacchi M., Hellstrom, J.C., Couchoud I., Monaco L., Ratti A., Martini F., Sarti L., 2020. An end to the Last Interglacial highstand before 120 ka: Relative sea-level evidence from Infreschi Cave (Southern Italy). Quaternary Science Reviews, 250, 106658.
-De Santis V., Scardino G., Scicchitano G., Meschis M., Montagna P., Pons-Branchu E., Ortiz J.E., Sánchez-Palencia Y., Caldara, M., 2023. Middle-late Pleistocene chronology of palaeoshorelines and uplift history in the low-rising to stable Apulian foreland: Overprinting and reoccupation. Geomorphology, 421, 108530.
-De Santis V., Montagna P., Scicchitano G., Mastronuzzi G., Pons-Brancu E., Scardino G., Ortiz J.E., Sanchez-Palencia Y., Torres T., Caldara M., in press. Two highstands during the Last Interglacial: insights from palaeoshorelines and marine terraced deposits along the Ionian coast of the Apulia region, Southern italy.
-Düsterhus A., Tamisiea M. E., Jevrejeva S., 2016. Estimating the sea level highstand during the Last Interglacial: a probabilistic massive ensemble approach. Geophysical Journal International, 206, 900–920.
-Kandiano E.S., Bauch H.A., Fahl,K. 2014. Last interglacial surface water structure in the western Mediterranean (Balearic) Sea: Climatic variability and link between low and high latitudes. Global and Planetary Change, 123, 67-76.
-Kopp R.E., Simons F.J., Mitrovica J.X., Maloof A.C., Oppenheimer M., 2013. A probabilistic assessment of sea level variations within the last interglacial stage. Geophysical Journal International 193, 711–716.
-Rohling E.J., Hibbert F.D., Grant K.M., Galaasen E.V., Irvali N., Kleiven H.F., Marino G., Ninnemann U., Roberts,A.P., Rosenthal Y., 2019. Asynchronous Antarctic and Greenland ice-volume contributions to the last interglacial sealevel highstand. Nature Communications 10, 5040.